JACS
JOURNAL OF THE AMERICAN CHEMICAL SOCIETY
Article
pubs.acs.org/JACS

Structural Insights into the Redox-Sensing Mechanism of MarR-Type Regulator AbfR

Guijie Liu,[†,‡,§] Xing Liu,[†,∥,§] Hongjiao Xu,[†,‡] Xichun Liu,[⊥] Hu Zhou,[∥] Zhen Huang,[#] Jianhua Gan,[▽] Hao Chen,[⊥] Lefu Lan,[†] and Cai-Guang Yang*[,†]

[†]Laboratory of Chemical Biology, State Key Laboratory of Drug Research, Shanghai Institute of Materia Medica, Chinese Academy of Sciences, Shanghai 201203, China

[‡]University of Chinese Academy of Sciences, Beijing 100049, China

[∥]CAS Key Laboratory of Receptor Research, Shanghai Institute of Materia Medica, Chinese Academy of Sciences, Shanghai 201203, China

[⊥]Coordination Chemistry Institute and State Key Laboratory of Coordination Chemistry, School of Chemistry and Chemical Engineering, Nanjing University, Nanjing 210093, China

[#]Department of Chemistry, Georgia State University, Atlanta, Georgia 30303, United States

[▽]School of Life Sciences, Fudan University, Shanghai 200433, China

Supporting Information

ABSTRACT: As a master redox-sensing MarR-family transcriptional regulator, AbfR participates in oxidative stress responses and virulence regulations in *Staphylococcus epidermidis*. Here, we present structural insights into the DNA-binding mechanism of AbfR in different oxidation states by determining the X-ray crystal structures of a reduced-AbfR/DNA complex, an overoxidized (Cys13-SO_2H and Cys13-SO_3H) AbfR/DNA, and 2-disulfide cross-linked AbfR dimer. Together with biochemical analyses, our results suggest that the redox regulation of AbfR-sensing displays two novel features: (i) the reversible disulfide modification, but not the irreversible overoxidation, significantly abolishes the DNA-binding ability of the AbfR repressor; (ii) either 1-disulfide cross-linked or 2-disulfide cross-linked AbfR dimer is biologically significant. The overoxidized species of AbfR, resembling the reduced AbfR in conformation and retaining the DNA-binding ability, does not exist in biologically significant concentrations, however. The 1-disulfide cross-linked modification endows AbfR with significantly weakened capability for DNA-binding. The 2-disulfide cross-linked AbfR adopts a very "open" conformation that is incompatible with DNA-binding. Overall, the concise oxidation chemistry of the redox-active cysteine allows AbfR to sense and respond to oxidative stress correctly and efficiently.

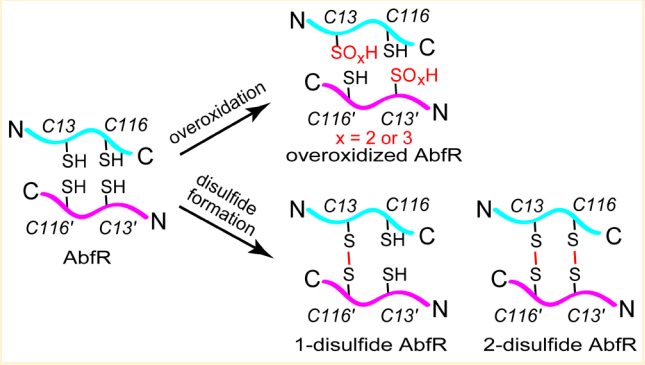

INTRODUCTION

Redox regulation involving reactive oxygen species (ROS) is a critical component of bacterial signaling through regulatory posttranslational modifications on thiol groups of redox-active and allosteric cysteines.[1,2] Oxidation-sensitive cysteines across bacterial proteomes have been profiled using the competitive activity-based protein profiling approach, indicating that pathogenic bacteria exhibit a complex, multilayered response to ROS challenge.[3] Indeed, many transcription factors could coordinate to regulate the expression of target genes in response to ROS,[4,5] and the regulation of different regulatory switches could be interconnected.[6] The key role of redox-sensing MarR-family transcriptional repressors including OhrR, OspR, AbfR, MgrA, HypR, SarZ, AsrR, MarR, MosR, MexR, YodB, and CymR has been shown to utilize oxidation chemistry of cysteines in order to sense oxidative stress and subsequently regulate bacterial responses among various pathogens.[7−20] In most cases, the first oxidation product of redox-active cysteine is sulfenic acid (Cys-SOH),[21,22] which is extremely active and either rapidly forms a disulfide bond by condensation with free sulfhydryl or is overoxidized to sulfinic acid (Cys-SO_2H) and sulfonic acid (Cys-SO_3H).[23,24] Several structural studies have characterized the intersubunit disulfide bond as well as the Cys-SOH intermediate.[10,25] Recently, the accommodations of other larger modification have been observed on the redox-active cysteine, which has also abolished DNA-binding, for example, phosphorylation and quinonization.[26,27] What is more, the oxidation state of redox-active cysteine has been shown to depend on the nature of the oxidant in the MarR-family

Received: November 8, 2016
Published: January 13, 2017

DOI: 10.1021/jacs.6b11438
J. Am. Chem. Soc. 2017, 139, 1598−1608

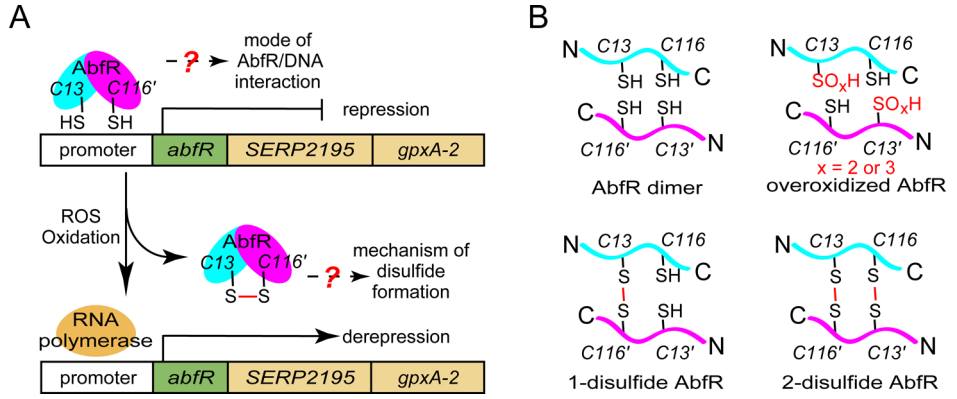

Figure 1. Oxidative regulation by AbfR through cysteine modifications. (A) Representation of the oxidation sensing and redox-regulation by AbfR in *S. epidermidis*. AbfR represses transcription of deoxidant genes without oxidative stress, but all the repressor while sensing oxidants, dissociates from promoter DNA, and activates transcription of deoxidant genes after oxidative stress. (B) The putative oxidative forms of AbfR dimers. The redox-active cysteine sensors could be converted into overoxidized species or intersubunit disulfide cross-links.

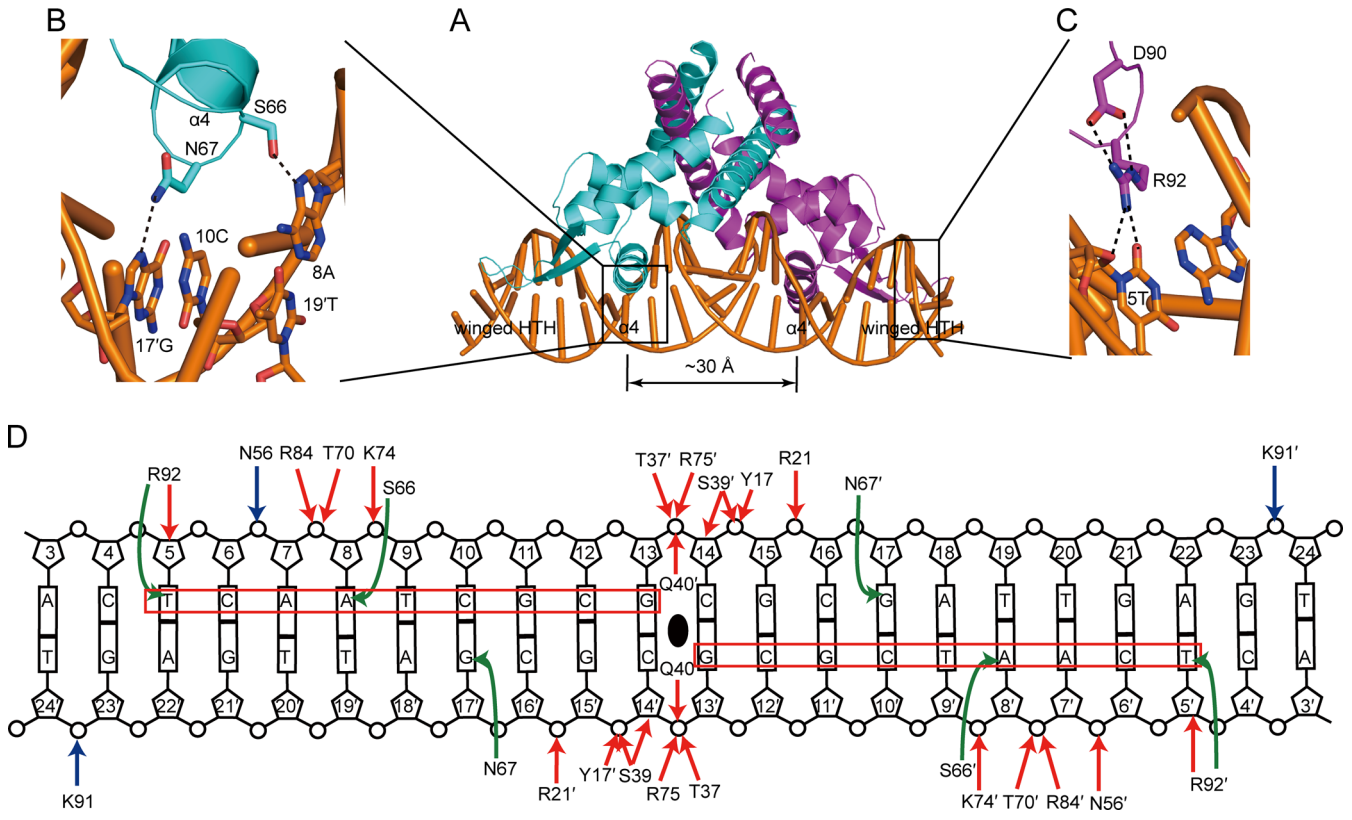

Figure 2. Crystal structure of reduced AbfR bound to promoter DNA. (A) Cartoon presentation of the structural complex of AbfR/DNA. One monomer is shown in cyan, the other in magenta, and the duplex DNA is colored in orange. The major-groove recognition helix α4, its 2-fold mate α4′, and the minor-groove binding elements winged HTH are indicated, respectively. (B) Close view of interactions between the helix α4 and DNA major-groove. Hydrogen-bonding is shown as black dashed lines, and the distance is within 3.2 Å. (C) Recognition of the DNA minor-groove by the winged HTH motif. (D) Schematic summary of major contacts between AbfR protein and DNA. Color codes are used as follows: the red arrow represents the protein side chain and phosphate backbone interaction, the blue arrow represents the protein main chain and phosphate backbone interaction, and the green arrow represents the base-specific protein−DNA contacts. The operator sequence specifically recognized by AbfR repressor is boxed in red.

transcriptional repressors.[28] For instance, linoleic acid hydroperoxide (LHP) predominantly causes the overoxidation of the sole redox-active cysteine to Cys-SO_2H and Cys-SO_3H in 1-Cys system *Bacillus subtilis* OhrR (*Bs*OhrR).[29] Given its unknown system of repair, the overoxidized *Bs*OhrR is also thought to function as a sacrificial regulator.

2-Cys-type *Staphylococcus epidermidis* AbfR is a master redox-sensing transcriptional regulator that participates in oxidative stress responses, bacterial aggregation, and biofilm formation.[19] We have shown that oxidative stress acts as a signal to modulate key virulence properties of *S. epidermidis* through the formation of Cys13-Cys116′ intersubunit disulfide bond in AbfR, a direct repressor of *abfR-SERP2195-gpxA* operon (Figure 1A). *SERP2195* encodes the E3 component of the α-keto acid dehydrogenase complex while *gpxA-2* encodes a glutathione peroxidase, both of which are involved in oxidative stress

DOI: 10.1021/jacs.6b11438
J. Am. Chem. Soc. 2017, 139, 1598−1608

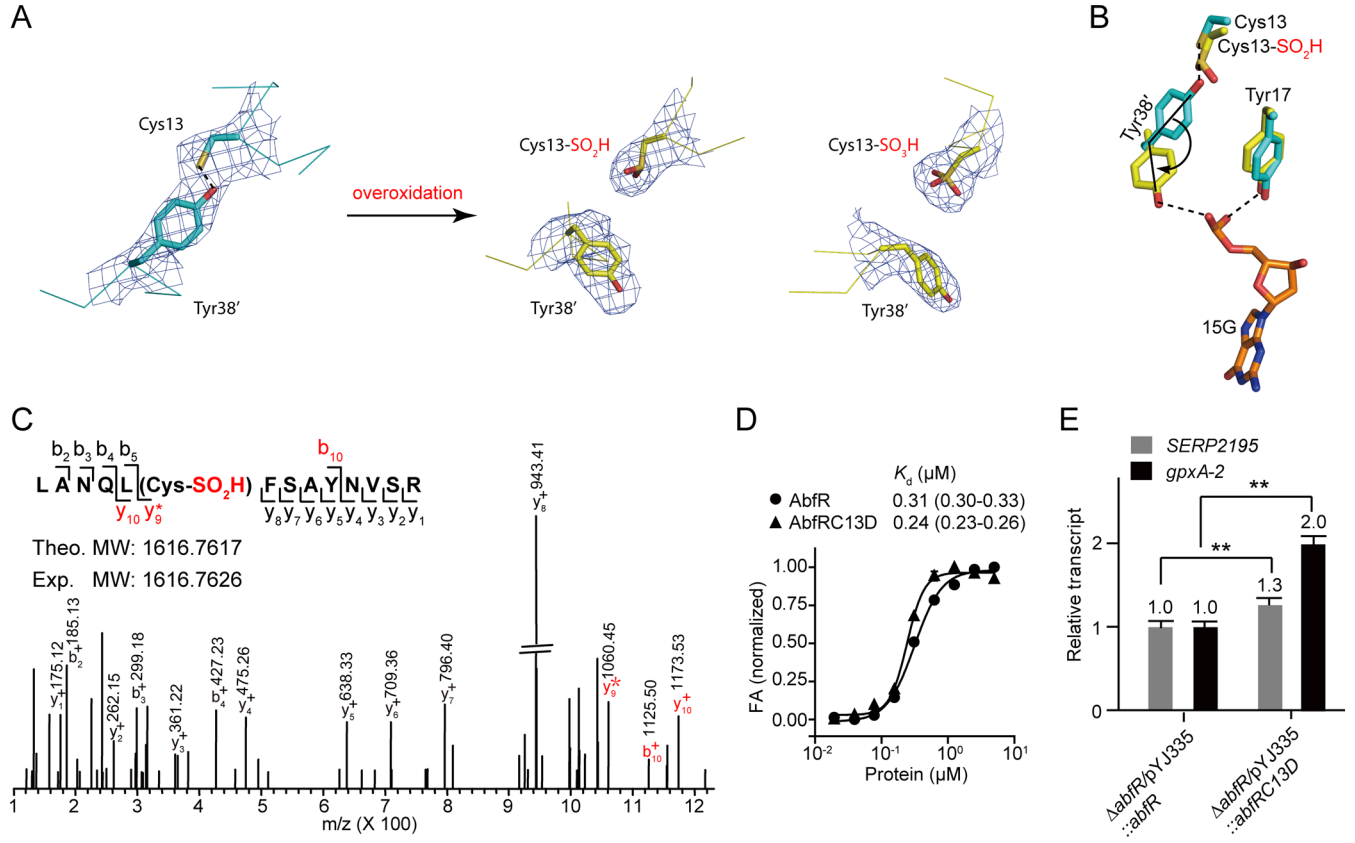

Figure 3. Characterization of the overoxidative modification on the redox-active Cys13. (A) Electron density map of the reduced and overoxidized cysteines, respectively. The σA weighted 2Fo-Fc map contoured at 1σ around Cys13 and Tyr38′ before and after overoxidation. The reduced AbfR is shown in cyan and the overoxidized AbfR in yellow. Atoms are colored in red (oxygen) and yellow (sulfur), and the density map is shown as blue mesh. The hydrogen-bonding is labeled with a black dashed line, and the distance is within 3.2 Å. (B) Local view of the structural alignment of the reduced and overoxidized AbfR/DNA complexes. The same color code is used as in A, and the DNA is in orange. The hydrogen-bonding of Tyr38′ and Tyr17 with phosphate backbone are indicated in black dashed lines, respectively. A curved arrow represents the conformational rotation of the Tyr38′ side chain after overoxidation. (C) LC−MS/MS identification of the overoxidative modification on the redox-active Cys13 in AbfR in vivo. Shown are mass spectrum and m/z peak assignment for the cysteine sulfinic acid. (D) Quantitative determination of the binding K_d for AbfR and AbfRC13D mimicking overoxidation of AbfR in FA, respectively. DNA at 20 nM was assayed. The normalized binding curve and K_d values in μM for each binding is given. All experiments were performed in triplicate, and 95% confidence intervals are given in brackets. (E) qRT-PCR analysis showing the relative transcript level of *SERP2195* and *gpxA-2* in Δ*abfR*/pYJ335::*abfR* and Δ*abfR*/pYJ335::*abfRC13D* without CHP treatment. All assays were performed in triplicate, and error bars represent the standard deviation. The significant differences ($P < 0.05$) between samples are denoted with asterisks.

response.[30,31] Two major questions remain unanswered, however. Does overoxidation occur on the redox-active cysteine sensor and how does it regulate DNA-binding? And what is the mechanism by which the formation of the disulfide bond in AbfR abolishes DNA-binding? Herein, we show structures of AbfR in different oxidation states (Figure 1B). On the basis of these structural studies in combination with biochemical evidence, our study reveals useful mechanistic insights into the formation of intersubunit disulfide modifications. In addition, we demonstrate that the formation of disulfide cross-links, but not the overoxidative modifications, efficiently abolishes the DNA-binding activity of AbfR.

RESULTS

Crystal Structure of the Reduced AbfR Bound to Promoter DNA. In order to investigate the mechanism of promoter-recognition by AbfR repressor, we crystallized the complex of reduced AbfR bound to promoter DNA in the presence of *tris*(2-carboxyethyl)phosphine (TCEP). A 24-bp DNA duplex containing the AbfR-recognizing sequence (TCAATCGCGCGCGATTGA) was cocrystallized with purified AbfR protein. The structure was determined to a resolution of 3.0 Å. Table S1 summarizes data collection and refinement statistics. As shown, the features of the protein−DNA interaction manner of AbfR are very similar to those of either *Mt*MosR or *Bs*OhrR (Figure 2A and S1).[16,32]

Our previous structural observations of the dimeric dimer of AbfR indicate that the conformation of AbfR is quite flexible. Comparison of the reduced AbfR in a DNA-free state to its DNA-binding state reveals a fairly large structural difference (Figure S2). The alignment of one dimer in the dimeric dimer of AbfR to the AbfR/DNA complex reveals a low degree of similarity with r.m.s.d. = 2.5 Å^2 for 198 corresponding Cα atoms (Figure S2A), while the other dimer to the AbfR/DNA complex shows a relatively high degree of similarity with r.m.s.d. = 1.6 Å^2 for 219 corresponding Cα atoms (Figure S2B), indicating that the DNA-free AbfR is incompatible with DNA-binding in high-affinity and thus likely binds to DNA via an induced fit. In the structure of the AbfR/DNA complex, the two recognition helices (α4 and α4′) in the winged HTH motif are separated by a distance of ∼30 Å (Figure 2A and S1C). This is consistent with the distance measured between the

DOI: 10.1021/jacs.6b11438
J. Am. Chem. Soc. 2017, 139, 1598−1608

recognition helices of *Mt*MosR and *Bs*OhrR bound to duplex DNA, respectively.[16,32] Two residues, Asn67 and Ser66, on the top tip position of helix α4 are situated in direct contact with bases in the DNA major-groove (Figure 2B). Hydrogen-bonding occurs between the amino side chain of Asn67 and N7 atom of guanine 17′. The hydroxyl group on the side chain of Ser66 directly forms hydrogen-bonding with the N7 atom of adenine 8. A major variation was also observed to occur thrice in the four dimeric AbfR/DNA complexes, which is the hydrogen-bonding between the carbonyl of Asn67 and N4 atom of cytosine 16′ in DNA major-groove (Figure S3). As the second DNA-binding element, the wing in the winged HTH motif directly interacts with bases in the DNA minor-groove. Arg92, which is located on the connecting loop region of the wing motif, participates in important hydrogen-bonding to thymine 5 nearby between guanidinium of Arg92 and both O2 and O4′ atoms of thymine 5. The neighboring residue Asp90 is always involved in the electrostatic interactions with Arg92 through the polar side-chains (Figure 2C). Besides the protein-base contacts, 24 residues in the AbfR dimer are involved in the formation of a large network of nonbase-specific contacts with the sugar phosphate backbone through electrostatic interactions. In total, 28 residues of the AbfR dimer make direct contact with DNA at least 32 times over a span of 20 nucleotides (Figure 2D and Table S2). These major interactions likely promote AbfR binding to duplex DNA in high-affinity as well as to stabilize the DNA-bound conformation of the reduced AbfR. Similar to *Bs*OhrR binding to *ohrA* operator DNA, the number of AbfR protein−DNA base contacts is fairly small and most of the central bases are not specifically recognized, however.[32] The sequence alignment clearly demonstrated that the base-binding motif Ser66 and Arg92 in AbfR are highly conserved among the MarR family proteins (Figure S4). However, it is unclear why the structural observations from complexes of both OhrR/DNA and AbfR/DNA fail to fully elucidate the DNA-binding specificities.[8,19] Taken together, this complex structure provides atomic-level insights into the mechanism of the reduced AbfR bound to DNA.

Structural Observation of Overoxidized AbfR. Interestingly, when the crystallization of AbfR/DNA complex was performed in the presence of DL-Dithiothreitol (DTT) as a reducing agent, we observed a structural complex of the overoxidized AbfR bound to the promoter DNA. The X-ray crystal structure was determined to a resolution of 3.0 Å. The final R_{work} and R_{free} were 22.6% and 27.2%, respectively (Table S1). We found both sulfinic and sulfonic acid modifications of Cys13, and the electron density across the overoxidation region was unambiguous (Figure 3A). There were three Cys13-SO_2H and five Cys13-SO_3H modifications existing in the four dimer/DNA complexes in the crystal lattice. One might have predicted a mixture of oxidation states for each of the Cys13 residues within each dimer, and the oxidation states of the redox-sensitive cysteine might depend on the oxidants. The overall architecture of the overoxidized AbfR is highly similar to the reduced AbfR in the conformation for DNA-binding (Figure 2A). Strikingly, the conformational orientations of the side chains of Tyr38 in the overoxidized AbfR/DNA complex sharply differ from those observed in the reduced AbfR bound to DNA. After the redox-active cysteines are oxidized to Cys-SO_2H or Cys-SO_3H, the two Tyr38 side chains (per dimer) move away from hydrogen-bonding with free thiols in Cys13 in order to avoid steric clash and come into contact with the phosphate backbone (Figure 3B and S5). All other structural elements that account for protein/DNA interactions remain intact, ensuring that the overoxidized AbfR retains its DNA-binding activity (Figure 2D). The conformational rotations of the Tyr38 side chains do not result in any major global changes, which is in line with the structural observation that over-oxidized AbfR is still binding to target DNA.

AbfR-Overoxidation Is Physiologically Unrelated. Inspired by the structural discovery of overoxidized AbfR, we speculate that the free redox-active cysteine could be overoxidized to either sulfinic acid or sulfonic acid (Figure 1B). We then treated the purified AbfR protein with and without Cumene hydroperoxide (CHP) and identified the products by using mass spectrometry analyses. The ESI-MS detection of full length protein typically detected species with the molecular weight of 17572.88, 17604.70, 35199.77 and 35257.90, and 35142.89, which could be putatively assigned to AbfR, overoxidized AbfR, 1-disulfide cross-linked AbfR, and 2-diuslfide cross-linked AbfR, respectively (Table S3). In order to characterize the protein fractions with the desired modification, we performed a trypsin-digestion assay coupled with LC−MS/MS analyses. Besides the reversible Cys13-Cys116′ disulfide characterized previously,[19] we have identified two new species of irreversible overoxidation on Cys13, Cys13-SO_2H and Cys13-SO_3H, respectively (Figure S6A−C). Similarly, when *S. epidermidis* was exposed to an environment of oxidative stress—CHP, for example—these overoxidative modifications on Cys13 in AbfR were also detectable (Figure 3C and S6D). Thus, the overoxidation could occur on AbfR both in vitro and inside the bacteria under oxidative stress.

It has been demonstrated that overoxidation of a single active site sufficed for the functional inactivation of *Bs*OhrR repressor in vitro.[33] However, the overoxidized AbfR could still bind to DNA in X-ray crystal structure. We validated whether the overoxidized AbfR impacts DNA-binding by utilizing Asp13 mutant (AbfRC13D) as a mimic of Cys13-SO_2H.[34] Using a fluorescence anisotropy (FA) analyses, we quantitatively measured the binding affinity between AbfRC13D and promoter DNA (K_d, 0.24 μM) (Figure 3D), which is quite similar to that of the wild-type AbfR binding to DNA (K_d, 0.31 μM). In order to examine whether Cys13 overoxidation could affect DNA-binding in vivo, we constructed an Δ*abfR*/pYJ335::*abfRC13D* strain and compared the in vivo transcript levels of the target genes in relation to the control Δ*abfR*/pYJ335::*abfR* strain, which could be a reflection on the DNA-binding ability in vivo. The transcript level of either *SERP2195* or *gpxA-2* in Δ*abfR*/pYJ335::*abfRC13D* strain was only 2-fold higher at most than that in the Δ*abfR*/pYJ335::*abfR* strain grown without CHP treatment (Figure 3E), suggesting that AbfRC13D most likely reserves the ability for DNA-binding in vivo. Together, these negligible differences on DNA-binding affinity in vitro and regulation of gene-transcription in vivo suggest that the overoxidized AbfR would not be physiologically related in response to oxidative stress.

In order to analyze in more detail the amount of the reversible and irreversible AbfR-oxidation after *S. epidermidis* was exposed to oxidative stress, we performed an iodoacetamide (IAM)-thiol-trapping assay coupled with AbfR-Western blot analyses.[13] The construct of Δ*abfR*/pYJ335::*flag-abfR* strain bears a FLAG tag at the C-terminal of *abfR* gene, which enabled us to enrich the AbfR protein in a way of pull-down assay. The pulled-down AbfR protein mainly migrates to the positions that correspond to the disulfide cross-linked dimer

DOI: 10.1021/jacs.6b11438
J. Am. Chem. Soc. 2017, 139, 1598−1608

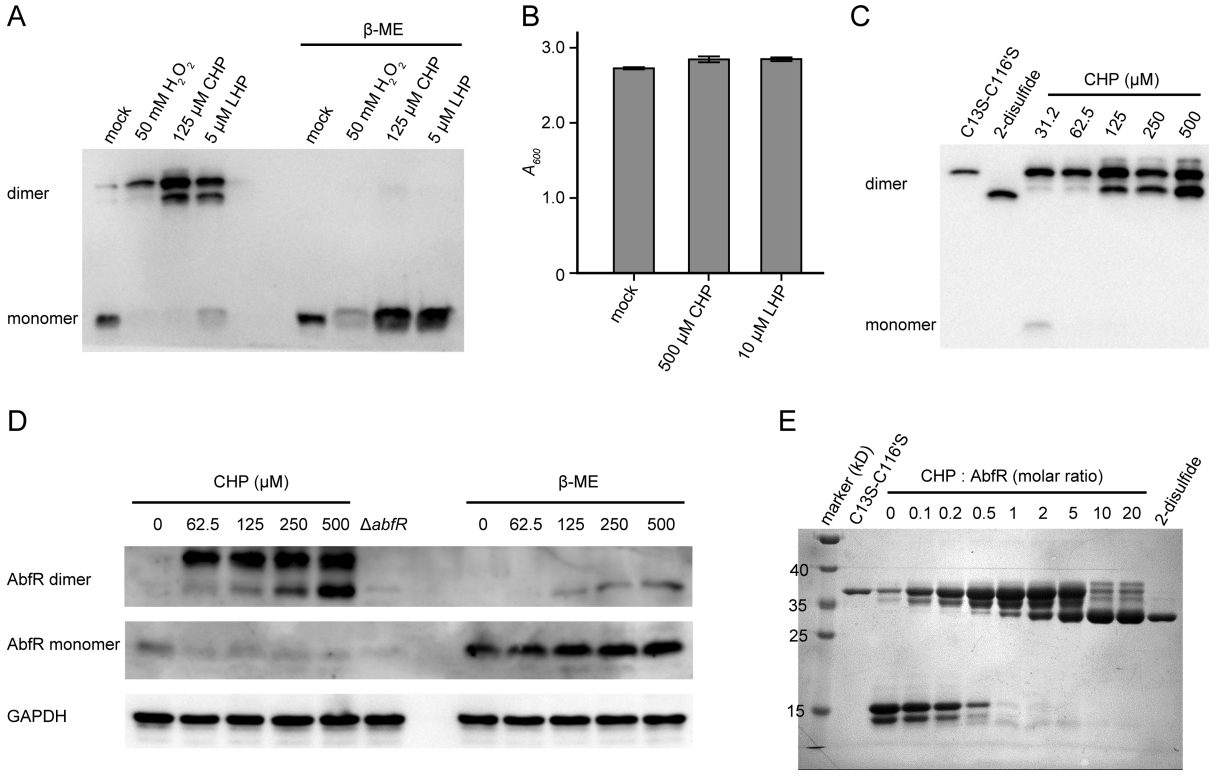

Figure 4. Illustration of the disulfide cross-linked AbfR modifications. (A) IAM-thiol-trapping assay with and without β-ME coupled with AbfR-Western blot analyses in order to analyze AbfR-oxidation after oxidative stress in vivo. The majority of the pulled-down AbfR migrated to the dimeric position in the nonreducing PAGE, which was steadily reduced to the monomeric state upon β-ME treatment. (B) The dosage of oxidants negligibly impacts *S. epidermidis* on growth. (C) AbfR-Western blot representative of the pulled-down AbfR-oxidation upon *S. epidermidis* (A_{600} 0.8) exposed to CHP at different concentrations. The purified samples of 1-disulfide cross-linked C13S−C116′S and 2-disulfide cross-linked AbfR were loaded as indicators. (D) IAM-thiol-trapping assay coupled with AbfR-Western blot analyses was run upon *S. epidermidis* (A_{600} 2.0) exposed to CHP for 15 min. The Δ*abfR*/pYJ335 strain was assayed and the GAPDH was loaded as internal reference. (E) CHP-promoted oxidation of purified AbfR protein in vitro. The migration positions of C13S−C116′S AbfR mutant and 2-disulfide cross-linked AbfR were representatives of the 1-disulfide and 2-disulfide cross-linked AbfR, respectively.

upon treatment with 50 mM hydrogen peroxide (H_2O_2), 125 μM CHP, or 5 μM LHP, respectively (Figure 4A). Of note, there were few monomeric AbfR bands left after oxidative stress, which indicates the formation of overoxidized AbfR is not in significant amount under the oxidative stresses tested. The dimeric AbfR bands could be completely reduced back to the monomeric positions by β-Mercaptoethanol (β-ME) treatment. These results indicate that the majority of the oxidative modifications on AbfR are reversible disulfide cross-links and that an irreversible modification, for example the overoxidized species, might not exist in biologically significant concentrations.

Biological Relevance of 1-Disulfide Cross-Linked AbfR. Next, we focused on characterization of the reversible disulfide modifications on the AbfR dimer. Since AbfR is more sensitive to organic peroxides than H_2O_2 as previously reported,[19] we utilized CHP and LHP as oxidants. The dosages of CHP and LHP are in the safe ranges for negligible impacts on the growth of *S. epidermidis* (Figure 4B). In order to have protein controls in hand, we performed DTNB (5,5′-dithiobis-(2-nitrobenzoic acid))-promoted oxidation of AbfRC13S and AbfRC116S mutants in order to generate 1-disulfide cross-linked AbfR mutant, CHP-promoted oxidation of wild-type AbfR in order to afford 1-disulfide cross-linked AbfR, and DTNB-promoted oxidation to 2-disulfide cross-linked AbfR, respectively. The qualities of these oxidized AbfR variants were confirmed by nonreducing SDS-PAGE analyses after chromatography purification (Figure S7). Intriguingly, FLAG-tagged pull-down enrichments coupled with AbfR-Western blot assay revealed that two distinct bands appeared in the size range corresponding to dimeric AbfR upon treatment of *S. epidermidis* with either 125 μM CHP or 5 μM LHP (Figure 4A). The position of the upper band is similar to the purified 1-disulfide cross-linked AbfR mutant (C13S−C116′S), while the migration position of the lower band is quite close to the 2-disulfide cross-linked AbfR (Figure 4C). In order to further investigate if the oxidation to the dimeric AbfR depends on oxidative strength, we treated *S. epidermidis* at the period of the exponential phase (A_{600} of 0.8) with CHP or LHP at different concentrations. The FLAG-tagged AbfR was enriched from CHP-treated *S. epidermidis* by way of pull-down experiments, while the whole lysate of LHP-treated *S. epidermidis* was directly subjected to AbfR-Western blot quantification. Obviously, there will always be two major dimeric AbfR bands, and the production of the lower 2-disulfide cross-linked AbfR will require an increased dosage of oxidants (Figure 4C and S8A). Similar phenomenon was observed when *S. epidermidis* at A_{600} of 2.0 was exposed to CHP at different concentrations, while the dimeric AbfR bands disappeared in Δ*abfR*/pYJ335 strain exposed to 500 μM CHP for 15 min (Figure 4D). In a previous characterization of oxidized AbfR by mass spectrometry, the intersubunit disulfide cross-link between Cys13 and Cys116′ was a major species, while the intersubunit "homo cross-link" at either Cys13-Cys13′ or Cys116-Cys116′ was not detectable.[19] In addition to

DOI: 10.1021/jacs.6b11438
J. Am. Chem. Soc. 2017, 139, 1598−1608

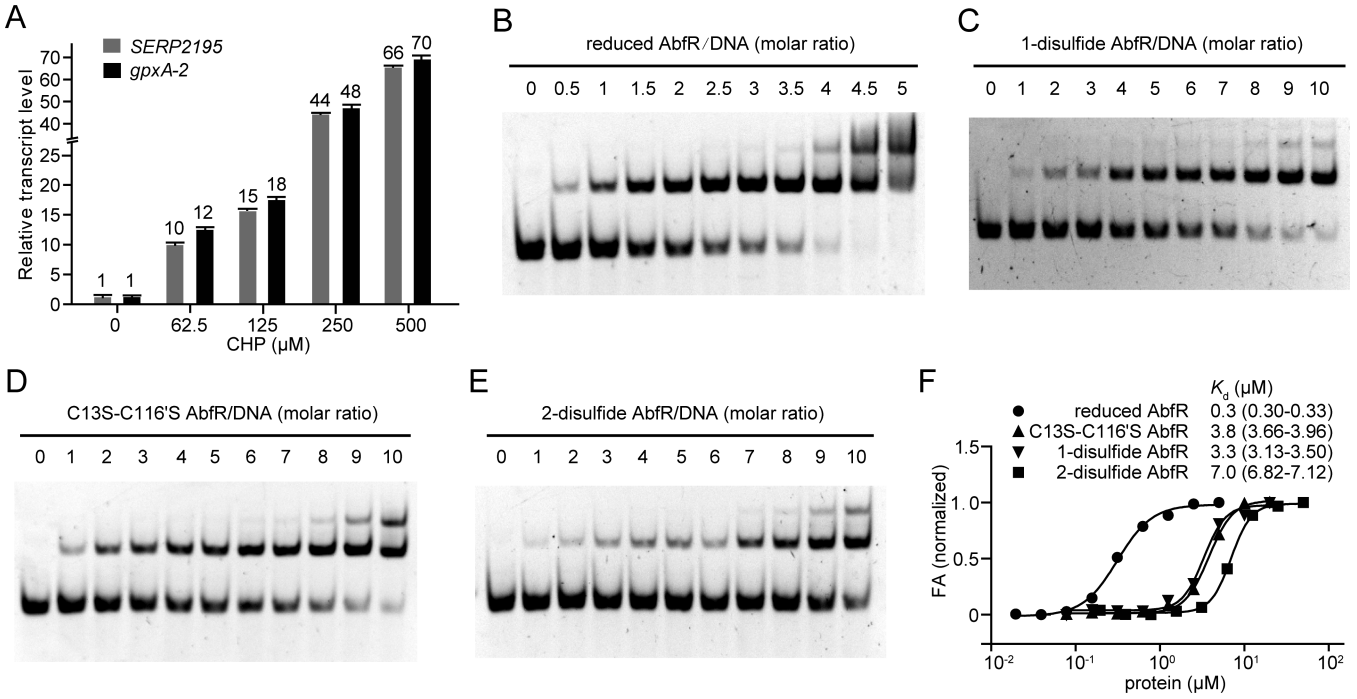

Figure 5. Redox-regulation and DNA-binding of disulfide cross-linked AbfR. (A) qRT-PCR analysis showing the relative transcript level of *SERP2195* and *gpxA-2* upon *S. epidermidis* strain exposed to CHP at different concentrations. All assays were performed in triplicate, and error bars represents the standard deviation. EMSA showing the DNA-binding of reduced AbfR (B), 1-disulfide cross-linked AbfR (C), C13S−C116′S AbfR mutant (D), and 2-disulfide cross-linked AbfR (E), respectively. DNA at 100 nM was assayed with the purified AbfR proteins. (F) Quantitative determination of the binding K_d for disulfide cross-linked AbfR in FA assay. DNA at 20 nM was assayed. The normalized binding curve and the K_d values in μM for each binding is given. All experiments were performed in triplicate, and 95% confidence intervals are given in brackets.

reference to the purified protein markers, we could speculate that the upper band is 1-disulfide cross-linked AbfR between Cys13 and Cys116′, while the lower is doubly cross-linked through the Cys13-Cys116′ and Cys13′-Cys116 bond.

In order to validate the biological existence of both 1-disulfide and 2-disulfide cross-linked AbfR, we performed in vitro oxidation of purified AbfR protein in the presence of CHP (Figure 4E). In the nonreducing SDS-PAGE, the 2-disulfide cross-linked AbfR migrated obviously faster than the C13S−C116′S 1-disulfide cross-linked mutant, which further demonstrates that the upper dimeric protein band from the pull-down assay could be the 1-disulfide cross-linked AbfR, and the lower dimeric band could be the 2-disulfide cross-linked AbfR (Figure 4C). Essentially, the formation of either 1-disulfide or 2-disulfide cross-linked AbfR might very well depend on the strength of oxidative stress and therefore, this oxidation chemistry could be stepwise. We treated wild-type AbfR protein by CHP or LHP in an IAM-thiol-trapping assay coupled with coomassie brilliant blue staining that is able to quantitatively demarcate the formation of the intersubunit disulfide cross-linked AbfR. Similar to the results of the in vivo pull-down assay, the oxidation of AbfR to disulfide modifications are the predominant chemistry in vitro. 1-Disulfide cross-linked AbfR dimer is the major product under relatively weak oxidative conditions: for example, the molar ratio of CHP versus AbfR is less than 5 or LHP versus AbfR is less than 1 (Figure 4E and S8B). When the oxidation stress becomes stronger, 1-disulfide cross-linked AbfR could be steadily converted to a 2-disulfide cross-linked dimer (Figure 4E and S8B). Together, these results indicated that AbfR was initially oxidized to 1-disulfide cross-link between Cys13 and Cys116′ under weaker oxidation stress, while the AbfR evolved to 2-disulfide cross-link when the oxidation stress became stronger, probably in a stepwise manner.

Functional Inactivation of 1-Disulfide Cross-Linked AbfR. We sought to investigate whether the generation of a 1-disulfide cross-link was sufficient to inactivate AbfR for DNA-binding. If so, the derepression of transcription for the *abfR-SERP2195-gpxA* operon could be partially activated under relative weak oxidation stress, by which AbfR was mainly oxidized to 1-disulfide cross-linked dimer. Quantitative real-time reverse transcription PCR (qRT-PCR) was performed in order to show the increased transcript level of both *SERP2195* and *gpxA-2* gene upon treating *S. epidermidis* with CHP in a dose-dependent manner (Figure 5A). The presence of CHP at 62.5 μM, by which AbfR was mainly oxidized to 1-disulfide cross-linked state as observed in the pull-down assay (Figure 4C), could result in more than a 10-fold increase of the transcript levels of *SERP2195* and *gpxA-2*, compared to what would occur in the absence of the oxidants. As expected, CHP stress at a relatively high concentration significantly activated the expression of the two target genes, which is a result of the negatively autoregulated expression of the *abfR* gene and accelerated oxidation to the disulfide cross-linked AbfR, thus causing a rapid accumulation inside bacteria.

Next, we tried to differentiate the impacts of 1-disulfide cross-linked AbfR from the 2-disulfide cross-linked AbfR on DNA-binding, by running electrophoretic mobility shift assay (EMSA) and FA assay. The result from EMSA displayed that oxidation of AbfR to the 1-disulfide cross-linked state already significantly weakened the capability for DNA-binding compared to the wild-type AbfR (Figure 5B,C). Similarly, the C13S−C116′S AbfR mutant displayed comparable DNA-binding affinity to the 1-disulfide cross-linked AbfR (Figure

DOI: 10.1021/jacs.6b11438
J. Am. Chem. Soc. 2017, 139, 1598−1608

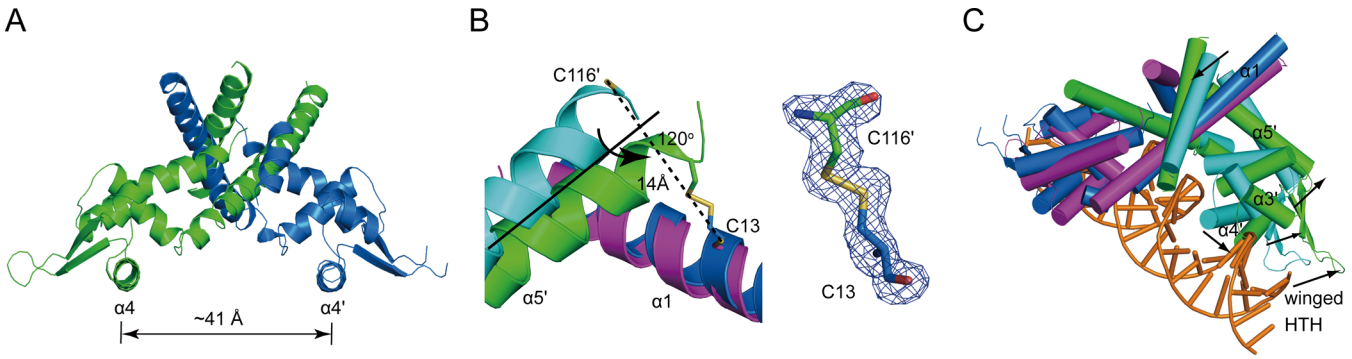

Figure 6. Crystal structure of 2-disulfide cross-linked AbfR. (A) Cartoon presentation of the dimeric AbfR bearing the intersubunit disulfide bonds. One monomer is shown in green, the other in marine. The two helices $\alpha4$ and $\alpha4'$ are separated by 41 Å in distance. (B) Conformational change before and after formation of disulfide bonds. The σA weighted Fo-Fc OMIT map contoured at 3σ around the disulfide bond between Cys13 and Cys116′ is shown. One monomer in the reduced AbfR is shown in cyan, the other in magenta. Atoms are colored in blue (nitrogen), red (oxygen), and yellow (sulfur), and distances are labeled as black dashed lines. The changes of residual position of Cys116′ and the angle of rigid body rotation of $\alpha5'$ are indicated. (C) The structural alignment of 2-disulfide cross-linked AbfR to AbfR/DNA complex in the reduced form. This is performed in PyMOL with a core r.m.s.d. of 4.4 Å^2 for 257 corresponding Cα atoms. The major motions of the motifs $\alpha4'$, $\alpha5'$, and the winged HTH in the 2-disulfide cross-linked AbfR are indicated by black arrows, which result in defective DNA-binding.

5C,D). The purified 2-disulfide cross-linked AbfR was assayed as a biological control, which further abolished the ability for DNA-binding (Figure 5E). Of note, it is unclear if the upper shifted protein/DNA band is an AbfR tetramer binding to DNA or nonspecific binding due to the high concentration of proteins assayed. In addition, it might be possible that additional binding sites exist in the operon, although the formation of tetramer as an additional mechanism for AbfR has not been reported yet, however. Consistently, FA for quantitative analyses revealed that the 1-disulfide cross-linked AbfR could significantly weaken the DNA-binding affinity over ~10-fold, while a decrease of over ~20-fold was observed when the purified 2-disulfide cross-linked AbfR was assayed (Figure 5F). Overall, the oxidative formation of 1-disulfide cross-link is sufficient for the functional inactivation of the dimeric AbfR for DNA-binding, while generation of the second disulfide further contributes to the attenuated activity for DNA-binding, and thus reflects on the derepression of the transcription of antioxidant genes.

Structural Insights into the 2-Disulfide Cross-Linked AbfR. In order to understand the mechanism of the formation of intersubunit disulfide cross-link that consequentially disrupts the DNA-binding conformation of AbfR, we sought to determine the crystal structure of the 2-disulfide formed AbfR. The structure was determined to a resolution of 2.05 Å (Figure 6A and Table S1). Electron density maps allow us to clearly assess the presence of the intersubunit disulfide bonds, as shown in the Fo-Fc OMIT density map contoured to 3.0 sigma (Figure 6B). In the structure of the reduced AbfR bound to duplex DNA, the two reactive cysteines that form the intersubunit disulfide bond upon oxidation are 14 Å apart (Sγ–Sγ) (Figure 6B). Meanwhile, the side chain of Cys116 is pointed away from Cys13 and exposed to solvent, thus indicating that a large structural change would be necessary in order for the formation of a disulfide bond between these two cysteine residues. Indeed, the alignment of the structure of 2-disulfide formed AbfR to either DNA-bound or DNA-free AbfR in the reduced form reveals remarkably large structural differences with r.m.s.d. = 4.4–5.6 Å^2 (Figure 6C and S9). Upon the formation of an intersubunit disulfide bond, the C-terminal half of the helix $\alpha5'$, where Cys116′ resides, rotates nearly 120° toward residue Cys13 of the opposing subunit (Figure 6B). In addition to this rotation, Cys116′ moves 7–9 Å in distance toward the N-terminus of helix $\alpha1$. Together these movements bring the thiol groups of these residues into proximity and permit the formation of the disulfide bond. Intriguingly, this rotation may act like a lever, causing both the winged-HTH motif ($\beta1$, $\beta2$, $\alpha3$, and $\alpha4$) of each subunit to rotate away from the other as a rigid body (Figure 6C). And the consequence of these rotations of the DNA-binding domains is an increased distance (41 Å) of the recognition helices ($\alpha4$) of each subunit (Figure 6A). Indeed, superimposition of the structures of disulfide-formed AbfR upon the AbfR/DNA complex reveals steric clashes between the disulfide-formed AbfR with DNA in the major-groove for DNA-binding (Figure 6C). Thus, 2-disulfide cross-linked AbfR dimer adopts a very "open" conformation that significantly abolishes DNA-binding.

DISCUSSION

The transcriptional factors of the MarR family, which feature a 1-Cys-type system and a 2-Cys-type system for oxidation chemistry, differ in their redox-sensing mechanisms. Generally, the initial oxidation of the redox-active cysteine sensor to the sulfenic acid intermediate might result in the disruption of the interaction network in the active site.[35] This disruption, however, is usually insufficient in order to inactivate the MarR repressor for DNA derepression.[36] In the 1-Cys-type system, the fate of the highly active Cys-SOH intermediate depends on the presence of thiols of low molecular weight and on the nature of the oxidant as well. For instance, the presence of thiols of low molecular weight leads to the rapid formation of a mixed disulfide.[36] On the other hand, LHP causes significant amounts of irreversible overoxidation to Cys-SO_2H and Cys-SO_3H acids.[29] In the 2-Cys-type system, the Cys-SOH intermediate could be rapidly quenched by the intersubunit allosteric cysteine. For example, the reversible redox-chemistry of the disulfide formation between the redox-active cysteine and the allosteric cysteine represents a major contribution to the oxidative response through the regulatory AbfR in *S. epidermidis*. The effect and mechanism of the oxidative modifications on the 2-Cys-type AbfR/DNA interaction have yet to be fully understood, however.

Similar to the other known 2-Cys-type redox-sensing MarR repressor, for example *Xc*OhrR,[10] the initial oxidation of the

DOI: 10.1021/jacs.6b11438
J. Am. Chem. Soc. 2017, 139, 1598–1608

redox-active cysteine in AbfR yields the sulfenic acid intermediate that could be captured immediately by the allosteric cysteine in order to form a disulfide cross-linked AbfR dimer. By using IAM-thiol-trapping assay coupled with AbfR-Western blot analyses, we were able to show the existence of 1-disulfide and 2-disulfide cross-linked AbfR dimers upon *S. epidermidis* treatment with oxidants. The formation of 1-disulfide cross-linked in AbfR is of biological relevance and functional significance, since it is sufficient to inactivate the repression of antioxidative gene due to the severely attenuated DNA-binding activity, thus suggesting that AbfR could utilize the 1-disulfide mechanism in order to sense and respond to the oxidant. Indeed, AbfR is not necessarily oxidized to 2-disulfide modification as the final destination, although it is in fact even more efficient for derepression. Of note, we can neither differentiate the contribution of each type of disulfide cross-linked AbfR, nor exactly determine the biological conditions necessary in order to generate each modification in vivo. The mixed disulfide cross-linked AbfR dimers could coexist as functionally inactive repressors in response to oxidative stress. Due to the global conformational changes, the covalently linked AbfR dimer adopts a very "open" conformation compared to the DNA-binding state, leading to the significant loss of DNA-binding activity. The formation of the intersubunit disulfide bond also fixes the conformation incompatible for DNA-binding, which, as an efficient response, quickly results in the derepression of multiple genes for antioxidation. Thus, coordination of the 1-disulfide pathway with 2-disulfide mechanism may allow AbfR to fine-tune gene transcription in response to oxidative stress.

In addition, we have expanded the characterization of the reversible disulfide-oxidation state of AbfR to the overoxidation of the redox-active cysteine in AbfR. The structural identification of a mixed cysteine sulfinic/sulfonic acid in the overoxidized AbfR/DNA complex adds new biochemical aspects in our understanding of the DNA-binding mechanism. Overoxidation, which requires successive oxidation, should indicate higher levels of external oxidants, during oxidative stress, for example, when activation of deoxidant genes might be more critical for cell survival. However, the overoxidized AbfR dimer does not rapidly dissociate from DNA like the disulfide cross-linked AbfR dimer does, since it is still capable of DNA-binding efficiently, where only the side chain of one tyrosine, and its 2-fold mate, switches from the hydrogen-bonding with the redox-active cysteine to a new position of contacting the phosphate backbone. This observation fits well the proposed domino effect that the oxidation of the redox-active cysteine to sulfenic acid intermediate would result in the repositioning of one tyrosine as the first domino in order to avoid subsequent steric clashes.[10,32] This small conformational change does not result in any major global changes in the AbfR/DNA complex, however, as the DNA-binding interaction is stabilized by other residues within the overoxidized AbfR dimer. Indeed, the AbfRC13D mimicking Cys13-SO_2H modification is still active for DNA-binding in vitro, showing a robust repression of the antioxidant gene expression in vivo. In addition, the overoxidized species of AbfR does not exist in biologically significant concentrations in vivo. Overall, the current data do not support the biological relevance of the overoxidized modifications in AbfR, meaning that overoxidation of the active cysteine sensor seems not to be an efficient redox-sensing mechanism in 2-Cys-type AbfR.

In summary, this study reveals the structural basis underlying the dissociation of DNA in the disulfide cross-linked conformation of AbfR versus reserved DNA-binding ability in the overoxidized conformation, which demonstrates why formation of the intersubunit disulfide bond, but not overoxidation, abolishes DNA-binding. In addition, we have characterized the 1-disulfide cross-linked AbfR dimer, which adds new aspects to our understanding of the redox-sensing mechanism of 2-Cys-type MarR repressors.

EXPERIMENTAL METHODS

Antibody and agents. Recombinant AbfR or GAPDH protein was overexpressed in *Escherichia coli*, purified by affinity chromatography, and utilized in order to raise polyclonal antibody in rabbit by Shanghai Immune Biotech Co. Ltd. CHP was purchased from Sigma. LHP was freshly generated by incubating 0.3 mM linoleic acid (Sigma) with soybean lipoxygenase (4000 U, Sigma) in 0.1 M sodium borate buffer (pH 9.0) at room temperature with vigorous stirring for 1 h.[29] The product was loaded onto an end-capped C18 reverse-phase column (Sepak cartridge), and LHP was eluted in 1.5 mL of methanol. The solution was stable for several months at −20 °C. The concentration of LHP was determined spectrophotometrically (λ = 234 nm, ε = 25,000 M^{-1} cm^{-1}). DNA oligos were purchased from Shanghai Generay Biotech Co., Ltd. and used without further purification.

Bacterial Strains, Plasmids, and Growth Condition. *S. epidermidis* was grown at 37 °C with aeration in tryptic soy broth (TSB, Oxoid) or BM medium (containing 10 g tryptone, 5 g yeast extract, 5 g NaCl, 1 g K_2HPO_4, and 1 g glucose per litter). For plasmid maintenance in *S. epidermidis*, the medium was supplemented with 10 μg/mL erythromycin. The *E. coli* strains used include DH5α for DNA manipulation and BL 21(DE3) for protein overexpression; both were routinely cultivated in Lysogeny Broth (LB, Difco). As previously described,[19] the *abfR* gene and its promoter were cloned into broad-host-range vector pYJ335, containing a C-terminus FLAG tag with the octapeptide sequence (N-Asp-Tyr-Lys-Asp-Asp-Asp-Asp-Lys-C) recognized by the M2 antibody (Sigma). The recombinant pYJ335 plasmid was introduced into the *Staphylococcus aureus* RN4220 strain, and then transferred into the *S. epidermidis* Δ*abfR* strain by electroporation to construct Δ*abfR*/pYJ335::*flag-abfR* strain.

Pull-Down of FLAG-Fusion AbfR. The Anti-FLAG M2Magnetic Beads (Sigma) were used to capture FLAG-fusion AbfR in Δ*abfR*/pYJ335::*flag-abfR*. The exponential-phase cells were harvested and resuspended in lysis buffer (50 mM Tris-HCl (pH 7.4), 150 mM NaCl, 0.5 mM EDTA, 1% TRITON X-100) with 50 mM IAM in order to alkylate all free thiols. After lysis by mechanical oscillation and centrifugation in order to remove all insoluble material, the protein supernatant was incubated with Anti-FLAG M2Magnetic beads for 1 h at room temperature with gentle mixing. Finally, the FLAG-fusion proteins were eluted by 0.1 M Glycine-HCl (pH 3.0) and immediately neutralized with 1.0 M Tris-HCl (pH 8.0).

Protein Expression and Purification. The expression and purification of AbfR was slightly modified from the published procedure.[19] A QuikChange Site-Directed Mutagenesis Kit (Stratagene) was used in order to construct the desired mutant plasmids. In order to facilitate the purification, *abfR* was cloned into pET30a vector. The *abfR*-coding region was PCR-amplified (PrimeSTAR, Takara) through the use of primers *abfR*-F and *abfR*-R. Then, the PCR product was digested with NcoI and *Bam*HI and ligated to the same sites in pET30a in order to create pET30a::*abfR*. PCR amplification and DNA sequencing verified the clones, which were subsequently transformed into a strain of BL21 Codon Plus (DE3) for AbfR expression. The *E. coli* cells were then grown in LB to A_{600} 0.6–0.8. Next, 0.5 mM of isopropyl β-D-1-thiogalactopyranoside (IPTG) was added. After incubation at 16 °C for 14 h, the culture was harvested. The pellet was stored at −80 °C. The cells were lysed at 4 °C by sonication in lysis buffer (20 mM Tris-HCl (pH 8.0), 200 mM NaCl, 0.1 mM EDTA, 10 mM β-ME, and 1 mM phenylmethylsulfonyl

DOI: 10.1021/jacs.6b11438
J. Am. Chem. Soc. 2017, 139, 1598−1608

fluoride (PMSF). Clarified cell lysate was subjected to Ni-NTA (HisTrap HP 5 mL, GE Healthcare), and the bound proteins were eluted with a linear gradient of elution buffer (20 mM Tris-HCl (pH 8.0), 200 mM NaCl, 0.5 M imidazole, 10 mM β-ME). A 14% SDS−polyacrylamide gel electrophoresis (SDS-PAGE) analysis was performed in order to identify the fractions that contained AbfR protein. The collected fractions were digested with thrombin (Sigma) at 4 °C for 12 h, and then the remaining His-AbfR protein was separated by Ni-NTA (HisTrap HP 5 mL, GE Healthcare). The His-tag free AbfR was collected and then buffer-exchanged to lysis buffer, and further purified by heparin and gel filtration (HiTrap heparin and HiLoad 16/600 Superdex 75 pg, GE Healthcare) with buffer (20 mM Tris-HCl (pH 8.0), 200 mM NaCl) in the presence of 2 mM DTT. Subsequently, the purified AbfR protein was concentrated to 10 mg/mL and used freshly.

Identification of AbfR-Oxidation by MS. The purified AbfR protein in its reduced form was buffer-exchanged to 20 mM Tris-HCl (pH 8.0), 200 mM NaCl by desalting at 4 °C. Then, AbfR protein was exposed to 50 μM CHP at 22 °C for 1 h, modified by 50 mM IAM in order to alkylate free thiols, and desalted. After sample preparation, the reduced and CHP-treated AbfR proteins were subjected to top-down MS analyses. A 1 μL injection volume of the desalted AbfR sample was loaded on a self-packed column (75 μm × 120 mm, 3 μm ReproSil-Pur C4 beads, 300 Å, Dr. MaischGmbH, Ammerbuch, Germany) at a flow rate of 300 nL/min. Mobile phase A consisted of 0.1% formic acid in water and mobile phase B consisted of 0.1% formic acid in acetonitrile. The proteins were eluted using a gradient (5−95% acetonitrile with 0.1% formic acid) over 20 min periods into a nano-ESI quadrupole Exactive (Q Exactive) mass spectrometer (Thermo Fisher Scientific). The mass spectrometer was operated in a continuous full scan mode (400−4000 m/z). Protein Deconvolution version (Thermo Fisher Scientific) was used to deconvolute multiply charged ESI spectra.

Bottom-up MS analyses was performed in order to identify overoxidation on AbfR. The protein was exposed to 50 μM CHP at 22 °C for 1 h. Then, the samples were treated with 50 mM IAM in order to alkylate any remaining free thiols, and then separated with nonreducing SDS-PAGE. The gels were stained with Coomassie blue and subsequently destained. The gel band containing AbfR protein was clipped out and cut into small pieces in a 1.5 mL microtube. To remove the staining dye, the chopped gels were washed three times with 50 mM NH_4HCO_3 in 30% acetonitrile by shaking at room temperature for 20 min. The gels were further incubated with 300 μL of acetonitrile at room temperature for 10 min. After acetonitrile was removed, the gel pieces were dried by Speed-Vac and rehydrated with 50 μL of trypsin solution (2.5 ng/μL trypsin in 50 mM NH_4HCO_3). The samples were digested for 16 h at 37 °C. Peptides were twice extracted with 85% acetonitrile and 0.1% trifluoroacetic acid. After the gel pieces were removed, the remaining solution was concentrated by Speed-Vac. The peptides were then redissolved in 30 μL of 0.1% formic acid for LC−MS/MS mass spectrometry analysis. The peptide mixtures were separated with a homemade reverse phase C18 column (150 mm × 75 μm, 3 μm ReproSil-Pur C18 beads, 120 Å, Dr. Maisch GmbH, Ammerbuch, Germany) at a flow rate of 300 nL/min. The mobile phase A was 0.1% formic acid in water, and B was acetonitrile containing 0.1% formic acid. The elution program consisted of a 5% mobile phase B held for 1 min, and then linearly increased to 30% mobile phase B within 45 min. The nano-LC effluent was subjected to an electrospray ionization linear ion trap (LTQ) Velso Pro-Orbitrap Elite mass spectrometer (Thermo Fisher Scientific). MS/MS spectra were acquired in a data-dependent acquisition mode that automatically selected and fragmented ten most intense peaks from each MS spectrum generated by high-energy collisional dissociation (HCD). For in vivo identification, a total of 200 mL of *S. epidermidis* culture in TSB at A_{600} 0.6 was treated with 250 μM CHP for 30 min. AbfR-FLAG was enriched through the use of anti-FLAG M2Magnetic Beads (Sigma), and analyzed as the in vitro procedure.

Preparation of Oxidized AbfR. The DTNB-promoted oxidation of AbfR for the formation of 2-disulfide cross-linked AbfR was performed according to the known procedure.[37] After the reducing agent was removed by desalting column (HiTrap, GE Healthcare), the AbfR protein was subjected to 5 equiv DTNB at room temperature for 1 h. Further purification was performed on monoQ (mono Q 10/100 GL). After the impurity proteins were thoroughly washed with equilibration buffer (20 mM Tris-HCl (pH 8.0), 250 mM NaCl), AbfR was collected with elution buffer (20 mM Tris-HCl (pH 8.0), 275 mM NaCl). A 14% nonreducing SDS-PAGE analysis was run in order to identify the fractions of 2-disulfide cross-linked AbfR proteins with highest purity. Similarly, the DTNB-promoted oxidation of AbfRC13S and AbfRC116S mutants (molar ratio = 1:1) was performed per the aforementioned procedure in order to form 1-disulfide cross-linked AbfR mutant. The formation of 1-disulfide cross-linked AbfR was achieved by CHP-promoted oxidation. After the reducing agent was removed by desalting column, the AbfR sample was subjected to oxidation in the presence of one equivalent CHP at room temperature for 15 min. Then, the reaction was quenched immediately by IAM alkylation in order to capture any remaining free thiols. Further purification was performed on monoQ (mono Q 10/100 GL).

AbfR-Western Blot. Proteins were loaded on a nonreducing 15% SDS-PAGE and separated by electrophoresis. The proteins from the gel were transferred electrophoretically for 0.5 h at 25 V by the semidry transfer cell to a nitrocellulose filter membrane (Merck Millipore). The membrane was blocked for 1 h at room temperature in 5% (m/v) skim milk dissolving in TBST buffer (20 mM Tris-HCl (pH 7.6), 150 mM NaCl, 0.1% Tween 20), and then hybridized for 1 h at room temperature with polyclonal antibodies diluted 1:2000 (anti-AbfR) or 1:5000 (anti-GAPDH) in 5% skim milk. After three washes in TBST buffer, the membrane was hybridized at room temperature with horseradish peroxidase conjugated to antirabbit antibodies (CoWin Biosciences) diluted 1:2000 in 5% skim milk. After three washes in TBST buffer, the bands were developed with the Tanon High-sig ECL Western Blotting Substrate (Tanon).

EMSA. A method slightly modified from the published method was used in order to perform EMSA.[19] Briefly, 20 μL of the mixture of duplex DNA (100 nM), purified AbfR proteins, and 50 pg/mL sonicated salmon sperm DNA in binding buffer (20 mM Tris-HCl (pH 7.4), 50 mM KCl, 5 mM $MgCl_2$) were let stand on ice for 15 min. After being mixed with 3 μL of loading buffer (20 mM Tris-HCl (pH 7.4), 150 mM KCl, 50% glycerol), the samples were run on a native polyacrylamide gel (6%) in 0.5 × TB buffer (50 mM Tris and 41.5 mM borate, pH 7.4) at 4 °C. The gel was stained in GelRed nucleic acid staining solution (Biotium) for 10 min, and then the DNA bands were visualized by gel exposure to UV light at a wavelength of 260 nm.

FA Assay. A 6-carboxyfluorescein-(6F-)-labeled DNA fragment containing the *abfR* operator site was generated by annealing 5′-6F-CTCCACCTCTTTTCAATCGCGCGCGATTGATTATAG-TATAAAATGACTCG-3′ and its unlabeled complementary strand. FA measurements were performed with 20 nM DNA and serial concentrations of AbfR in 50 μL of 50 mM HEPES (pH 7.4). After incubation for 15 min at 22 °C, FA was measured on an EnVision Multilabel Plate Reader (PerkinElmer) with a wavelength of 480 nm for excitation and 520 nm for emission, respectively. The concentration of AbfR/DNA complex is lesser than 3.26% and 4.60% of total protein concentration for wild-type AbfR and C13D mutant, respectively, which ruled out "receptor depletion". The normalized FA, which stands for the bound AbfR/DNA complex, is plotted as a function of AbfR concentration using a logarithmic scale. The K_d values were then calculated by using nonlinear regression analyses using GraphPad Prism 5.0. Each reaction was performed in triplicate.

qRT-PCR. RNA isolation and qRT-PCR were carried out as previously described.[19] Briefly, total RNA was extracted from exponential-phase cells (A_{600} 0.8, according to *S. epidermidis* 1457) with a QIAGEN RNAeasy Mini Kit. 500 ng of total RNA was reverse-transcribed by using the PrimeScript RT reagent Kit (Takara) according to the manufacturer's instructions. The qRT-PCR reactions were performed on the Prism 7500 real-time PCR system (ABI). The *gyrB* gene was chosen as an internal control. The transcript level of *gyrB* was measured at various growth stages and was observed to be consistent. Primer pairs, RT-SE2195F/*RT*-SE2195R and RT-gpxAF/

DOI: 10.1021/jacs.6b11438
J. Am. Chem. Soc. 2017, 139, 1598−1608

RT-gpxAR, were used for the detection of *SERP2195* and *gpxA-2*, respectively. The experiments were performed in triplicate as biological repeats, and transcript levels were calculated relative to those of *gyrB*.

Crystallization and Structure Determination. Several oligodeoxynucleotides containing the sequence of the *abfR*-operator binding site and ranging from 20- to 30-bp in length were screened for crystallization with 10 mg/mL of AbfR protein in buffer (20 mM Tris-HCl (pH 8.0), 200 mM NaCl) containing 1 mM TCEP or 2 mM DTT. Diffraction-quality crystals were grown in hanging drops by mixing AbfR and a 24-bp DNA with 5′-T A overhangs at a molar ratio of 1:2 (protein dimer: DNA) in a precipitant of 100 mM sodium cacodylate (pH 6.5), 100 mM NaCl, 50 mM $MgCl_2$, and 12% polyethylene glycol 5000 at 4 °C. Crystals were grown within several days and flash-frozen in liquid nitrogen following cryoprotection with a reservoir solution containing an extra 20% glycerol.

Crystallization of 2-disulfide cross-linked AbfR was performed using the hanging-drop vapor diffusion method at 20 °C. The final optimized crystallization condition consists of 1 μL of 2-disulfide formed AbfR dimer at 5 mg/mL and 1 μL of a precipitation solution (8% v/v Tacsimate pH 8.0, 20% w/v polyethylene glycol 3350). High-quality crystals were grown within several days and were flash-frozen in liquid nitrogen following cryoprotection with the reservoir solution containing an extra 20% glycerol.

Diffraction data were collected at the Shanghai Synchrotron Radiation Facility (SSRF) beamline 17U. All X-ray data were processed using the HKL2000 program[38] and converted to structural factors within the CCP4.[39] The structures were solved by molecular replacement in Phaser[40] by using one dimer in the reduced AbfR structure (PDB entry 4HBL) as the search model.[32] The model was manually built using COOT[41] and computational refinement was carried out in the program PHENIX.[42] Molecular graphics were prepared with PyMOL.[43]

■ ASSOCIATED CONTENT

Supporting Information

The Supporting Information is available free of charge on the ACS Publications website at DOI: 10.1021/jacs.6b11438.

The structures of AbfR/DNA complexes, structural alignments of AbfR in different states, MS analysis of oxidative modifications on AbfR, PAGE analyses of oxidized AbfR proteins, X-ray crystal data collection and refinement statistics, and hydrogen-bonding pairs in AbfR/DNA complexes (PDF)

■ AUTHOR INFORMATION

Corresponding Author

*yangcg@simm.ac.cn

ORCID

Hao Chen: 0000-0001-8937-4946

Cai-Guang Yang: 0000-0001-5778-4422

Author Contributions

§G.L. and X.L. contributed equally.

Notes

The authors declare no competing financial interest.

Atomic coordinates and structure factors have been deposited in the Protein Data Bank (PDB, www.pdb.org) under accession ID code 5HLG for the complex structure of AbfR/DNA, 5HLH for the complex structure of overoxidized AbfR/DNA, and 5HLI for the structure of the 2-disulfide formed AbfR, respectively.

■ ACKNOWLEDGMENTS

This work was supported by grants from the National Natural Science Foundation of China (90913010, 81661138004) to C.Y., (31500110) to X.L., and (20721002, 91013009) to H.C., the National Key Research and Development Projects (2016YFA0501500) to C.Y. and (2012CB933802, 2015CB856303) to H.C.. We thank the beamline scientists at SSRF (BL17U) for their support in data collection, and S.F. Reichard for editing the manuscript.

■ REFERENCES

(1) Vázquez-Torres, A. *Antioxid. Redox Signaling* **2012**, *17*, 1201.

(2) Antelmann, H.; Helmann, J. D. *Antioxid. Redox Signaling* **2011**, *14*, 1049.

(3) Deng, X.; Weerapana, E.; Ulanovskaya, O.; Sun, F.; Liang, H.; Ji, Q.; Ye, Y.; Fu, Y.; Zhou, L.; Li, J.; Zhang, H.; Wang, C.; Alvarez, S.; Hicks, L. M.; Lan, L.; Wu, M.; Cravatt, B. F.; He, C. *Cell Host Microbe* **2013**, *13*, 358.

(4) Dubbs, J. M.; Mongkolsuk, S. *J. Bacteriol.* **2012**, *194*, 5495.

(5) Grove, A. *Curr. Biol.* **2013**, *23*, R142.

(6) Atichartpongkul, S.; Vattanaviboon, P.; Wisitkamol, R.; Jaroensuk, J.; Mongkolsuk, S.; Fuangthong, M. *PLoS One* **2016**, *11*, e0161982.

(7) Chen, H.; Hu, J.; Chen, P. R.; Lan, L.; Li, Z.; Hicks, L. M.; Dinner, A. R.; He, C. *Proc. Natl. Acad. Sci. U. S. A.* **2008**, *105*, 13586.

(8) Fuangthong, M.; Helmann, J. D. *Proc. Natl. Acad. Sci. U. S. A.* **2002**, *99*, 6690.

(9) Panmanee, W.; Vattanaviboon, P.; Poole, L. B.; Mongkolsuk, S. *J. Bacteriol.* **2006**, *188*, 1389.

(10) Newberry, K. J.; Fuangthong, M.; Panmanee, W.; Mongkolsuk, S.; Brennan, R. G. *Mol. Cell* **2007**, *28*, 652.

(11) Lan, L.; Murray, T. S.; Kazmierczak, B. I.; He, C. *Mol. Microbiol.* **2010**, *75*, 76.

(12) Chen, P. R.; Bae, T.; Williams, W. A.; Duguid, E. M.; Rice, P. A.; Schneewind, O.; He, C. *Nat. Chem. Biol.* **2006**, *2*, 591.

(13) Palm, G. J.; Khanh Chi, B.; Waack, P.; Gronau, K.; Becher, D.; Albrecht, D.; Hinrichs, W.; Read, R. J.; Antelmann, H. *Nucleic Acids Res.* **2012**, *40*, 4178.

(14) Chen, P. R.; Nishida, S.; Poor, C. B.; Cheng, A.; Bae, T.; Kuechenmeister, L.; Dunman, P. M.; Missiakas, D.; He, C. *Mol. Microbiol.* **2009**, *71*, 198.

(15) Lebreton, F.; van Schaik, W.; Sanguinetti, M.; Posteraro, B.; Torelli, R.; Le Bras, F.; Verneuil, N.; Zhang, X.; Giard, J. C.; Dhalluin, A.; Willems, R. J.; Leclercq, R.; Cattoir, V. *PLoS Pathog.* **2012**, *8*, e1002834.

(16) Brugarolas, P.; Movahedzadeh, F.; Wang, Y.; Zhang, N.; Bartek, I. L.; Gao, Y. N.; Voskuil, M. I.; Franzblau, S. G.; He, C. *J. Biol. Chem.* **2012**, *287*, 37703.

(17) Chi, B. K.; Albrecht, D.; Gronau, K.; Becher, D.; Hecker, M.; Antelmann, H. *Proteomics* **2010**, *10*, 3155.

(18) Ji, Q.; Zhang, L.; Sun, F.; Deng, X.; Liang, H.; Bae, T.; He, C. *J. Biol. Chem.* **2012**, *287*, 21102.

(19) Liu, X.; Sun, X.; Wu, Y.; Xie, C.; Zhang, W.; Wang, D.; Chen, X.; Qu, D.; Gan, J.; Chen, H.; Jiang, H.; Lan, L.; Yang, C. G. *J. Biol. Chem.* **2013**, *288*, 3739.

(20) Hao, Z.; Lou, H.; Zhu, R.; Zhu, J.; Zhang, D.; Zhao, B. S.; Zeng, S.; Chen, X.; Chan, J.; He, C.; Chen, P. R. *Nat. Chem. Biol.* **2014**, *10*, 21.

(21) Gupta, V.; Carroll, K. S. *Biochim. Biophys. Acta, Gen. Subj.* **2014**, *1840*, 847.

(22) Furdui, C. M.; Poole, L. B. *Mass Spectrom. Rev.* **2014**, *33*, 126.

(23) Hochgrafe, F.; Mostertz, J.; Pother, D. C.; Becher, D.; Helmann, J. D.; Hecker, M. *J. Biol. Chem.* **2007**, *282*, 25981.

(24) Lo Conte, M.; Carroll, K. S. *J. Biol. Chem.* **2013**, *288*, 26480.

(25) Poor, C. B.; Chen, P. R.; Duguid, E.; Rice, P. A.; He, C. *J. Biol. Chem.* **2009**, *284*, 23517.

DOI: 10.1021/jacs.6b11438
J. Am. Chem. Soc. 2017, 139, 1598−1608

(26) Sun, F.; Ding, Y.; Ji, Q.; Liang, Z.; Deng, X.; Wong, C. C.; Yi, C.; Zhang, L.; Xie, S.; Alvarez, S.; Hicks, L. M.; Luo, C.; Jiang, H.; Lan, L.; He, C. *Proc. Natl. Acad. Sci. U. S. A.* **2012**, *109*, 15461.
(27) Ji, Q.; Zhang, L.; Jones, M. B.; Sun, F.; Deng, X.; Liang, H.; Cho, H.; Brugarolas, P.; Gao, Y. N.; Peterson, S. N.; Lan, L.; Bae, T.; He, C. *Proc. Natl. Acad. Sci. U. S. A.* **2013**, *110*, 5010.
(28) Duarte, V.; Latour, J. M. *Mol. BioSyst.* **2010**, *6*, 316.
(29) Soonsanga, S.; Lee, J. W.; Helmann, J. D. *Mol. Microbiol.* **2008**, *68*, 978.
(30) Tretter, L.; Adam-Vizi, V. *Philos. Trans. R. Soc., B* **2005**, *360*, 2335.
(31) Moore, T. D.; Sparling, P. F. *J. Bacteriol.* **1996**, *178*, 4301.
(32) Hong, M.; Fuangthong, M.; Helmann, J. D.; Brennan, R. G. *Mol. Cell* **2005**, *20*, 131.
(33) Eiamphungporn, W.; Soonsanga, S.; Lee, J. W.; Helmann, J. D. *Nucleic Acids Res.* **2009**, *37*, 1174.
(34) Voss, J.; Sun, J.; Venkatesan, P.; Kaback, H. R. *Biochemistry* **1998**, *37*, 8191.
(35) Soonsanga, S.; Fuangthong, M.; Helmann, J. D. *J. Bacteriol.* **2007**, *189*, 7069.
(36) Lee, J. W.; Soonsanga, S.; Helmann, J. D. *Proc. Natl. Acad. Sci. U. S. A.* **2007**, *104*, 8743.
(37) Chen, H.; Yi, C.; Zhang, J.; Zhang, W.; Ge, Z.; Yang, C. G.; He, C. *EMBO Rep.* **2010**, *11*, 685.
(38) Otwinowski, Z.; Minor, W. *Methods Enzymol.* **1997**, *276*, 307.
(39) Collaborative Computational Project. *Acta Crystallogr., Sect. D: Biol. Crystallogr.* **1994**, *50*, 760.
(40) Read, R. J. *Acta Crystallogr., Sect. D: Biol. Crystallogr.* **2001**, *57*, 1373.
(41) Emsley, P.; Cowtan, K. *Acta Crystallogr., Sect. D: Biol. Crystallogr.* **2004**, *60*, 2126.
(42) Murshudov, G. N.; Vagin, A. A.; Dodson, E. J. *Acta Crystallogr., Sect. D: Biol. Crystallogr.* **1997**, *53*, 240.
(43) DeLano, W. L. *The PyMOL Molecular Graphics System*; DeLano Scientific, 2002.

DOI: 10.1021/jacs.6b11438
J. Am. Chem. Soc. 2017, 139, 1598−1608